Studies on Resolving Injected Sterile Neutrino Oscillation Signals by Observing Muon Neutrino Disappearance with the Short Baseline Neutrino Program

Davio Cianci
University of Chicago

October 16, 2014

MicroBooNE and LAr1–ND

MicroBooNE–DocDB 3826, SBN–DocDB 148 (v0-1)

ABSTRACT

This tech-note will demonstrate how the detector setup of the Short Baseline Program will expand the current limits in ν_μ disappearance studies. The signal injection plots will both illustrate and heighten our understandings of the sensitivity plots shown in earlier studies. While the signal injection plots signify a great improvement, they also present the limitations in our approach to confidence level cuts, requiring a more statistical approach to account for the fluctuation of the best-fit point for signals in low-sensitivity regions of the Δm^2_{41}–$\sin^2(2\theta_{\mu\mu})$ parameter space.

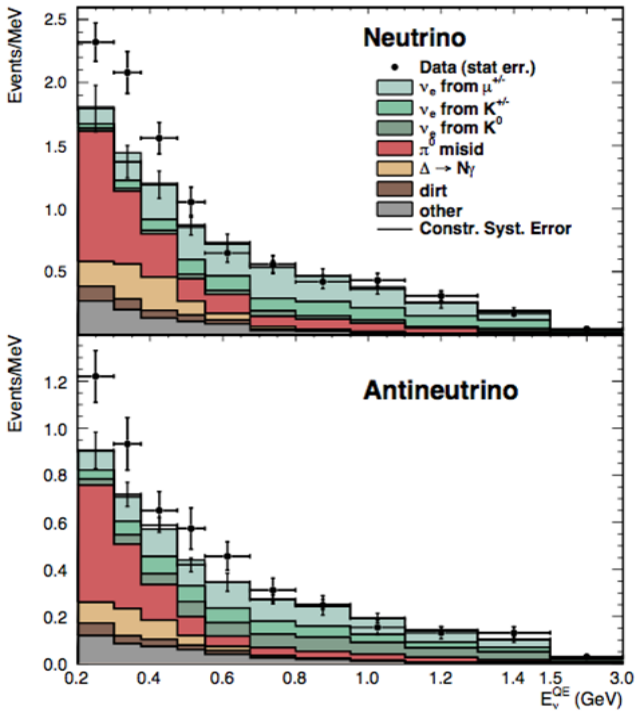

FIG. 1: *MiniBooNE ν_e findings, illustrating detection of an excess of both electron neutrinos and anti-neutrinos in the Fermilab Booster Beam [1].*

I. EXPERIMENTAL ANOMALIES: MINIBOONE + LSND

The original impetus for these studies, as well as the Booster neutrino program, stemmed from an electron neutrino excess detected by LSND [2] and further by MiniBooNE [1].

One proposed solution is that there exist more than the three flavors of neutrinos described in the standard model. These new hypothetical neutrinos have been labeled sterile neutrinos for their inability to interact even via the weak interaction, making them very difficult to detect. With this solution in consideration, the observation in LSND and MiniBooNE could be explained by muon neutrinos mixing through an additional sterile neutrino state resulting in more electron neutrinos than a three-neutrino oscillation model would have allowed. As it stands, the three-neutrino model of oscillation contains an $\frac{L}{E}$ component which should suppress ν_e appearance almost entirely at short baselines and accelerator energies.

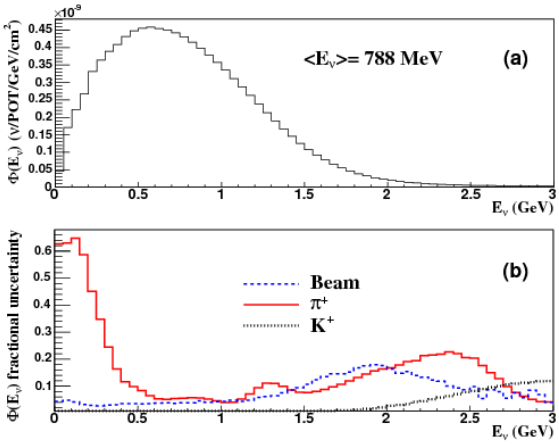

FIG. 2: *Uncertainty due to the neutrino flux found in MiniBooNE [3].*

II. ν_μ DISAPPEARANCE

Approximately 99% [4] of the beam is comprised of muon neutrinos with electron neutrinos making up the rest. This makes ν_e appearance far more noticeable, particularly in detectors with less resolution. Difficulty also arises when one considers uncertainties in the booster beam flux. From Fig. 2 we see that even at its lowest, there is a beam uncertainty of close to 9% in a single detector. This uncertainty is relatively insignificant with the low presence of electron neutrinos, but it makes muon neutrino disappearance much harder to observe down with confidence.

The main analysis of the Short Baseline Neutrino program is of ν_e appearance, but in order to interpret it as an oscillation with sterile neutrinos, one needs to observe the disappearance of muon neutrinos with equal or greater probability. A ν_e appearance study observes particles that begin as ν_μ, oscillate to some other particle and then end as a ν_e. The difficulty comes from that middle step, which could have any number of potential oscillations. Different numbers of sterile neutrinos would all provide different results in the study. A disappearance study, however, simply observes particles that begin as ν_μ and oscillate into anything else. This makes fewer initial assumptions, but when paired with a ν_e appearance analysis gains the most strength. If more muon neutrinos disappear than electron neutrinos appear, it raises more interesting questions and lends further evidence towards a non-standard model solution.

The ν_μ disappearance formula is given by [5]:

$$P(\nu_\mu \to \nu_x) = 1 - \sin^2(2\theta_{\mu\mu}) \sin^2(1.27\Delta m^2_{41} \frac{L_\nu}{E_\nu}). \quad (1)$$

To constrain flux uncertainties, the short baseline program plans to install a near detector, LAr1–ND to be placed directly in front of the beam at 100m from the neutrino target. This detector's findings will allow us to constrain the beam and effectively lower this flux uncertainty. Pairing this with MicroBooNE and the upcoming T–600 detector allows us to use these statistics to constrain data in order to potentially observe ν_μ disappearance with greater confidence.

III. SENSITIVITY CURVES

We want to know how well we can constrain the parameters of sterile neutrino oscillation through observation of ν_μ disappearance with our detector setup of LAr1–ND (100m), MicroBooNE (470m), and T–600 (600m).

The current state of the art are sensitivity studies which compare a predicted sterile neutrino oscillations over a phase space of Δm^2_{41} and $\sin^2(2\theta_{\mu\mu})$ with a null hypothesis and record our ability to resolve each signal. In order to do these studies, we store the energy distributions for the null hypothesis and predicted oscillations into vector, calculate the χ^2 value for each prediction, using a covariance matrix to determine uncertainties and we draw contours on the phase space to correspond to cuts. The process results in a χ^2 value for each point in the phase space. Sensitivity curves are simply cross sectional cuts of this χ^2 surface at different confidence levels.

The χ^2 value for each point is given by:

$$\chi^2 = (E_{null} - E_{pred})_i Cov^{-1}_{ij} (E_{null} - E_{pred})_j \tag{2}$$

where E_{null} is the null hypothesis vector, E_{pred} is the prediction vector and Cov is the covariance matrix. With an array of χ^2 values for each point in the Δm^2_{41}–$\sin^2(2\theta_{\mu\mu})$ phase space, we run a one-directional Raster scan to draw curves for each confidence level. Since we scan only from one side, we only see variation in the Δm^2_{41} parameter, so we use a one-sided χ^2 distribution with one degree of freedom. The code goes through the χ^2 of each Δm^2_{41} point and finds the cut-offs for 5σ ($\chi^2 = 23.40$), 3σ ($\chi^2 = 7.74$), and 90% Confidence ($\chi^2 = 1.64$) [6].

The null hypothesis is an energy spectrum of ν_μ under the assumption that there is no oscillation to sterile neutrinos. It is constructed by Monte Carlo for each of the three detectors in the setup.

Each prediction vector is built from this null hypothesis before subtracting the proportion

of muon neutrinos that will have oscillated to sterile neutrinos with oscillation parameters given by each point in the phase space, using Eq. 1.

With a full nominal uncertainty matrix, we wish to incorporate uncertainty in the beam flux. Similar uncertainty matrices are built for different systematic fluctuations in the beam makeup [8]. To get the components of the final covariance matrix, we use Eq. 3 for each n and average over $N = 1000$ systematic fluctuations.

$$E_{ij} = (Nom - Sys)_i (Nom - Sys)_j. \tag{3}$$

As part of the shape-only analysis, all components are factorized and scaled to the null hypothesis in the near detector to remove normalization information. The statistical uncertainty is then added along the diagonal.

Limitations in our knowledge of the normalization uncertainties, particularly with regards to cross-section normalizations, have prevented us from having implemented any into our code. We instead opt to disregard normalization information altogether and run a purely shape-only analysis. Without proper knowledge about these cross sections, our results would be overly optimistic. By cutting them out and limiting ourselves to only the shape information of these energy spectra, we get more realistic sensitivity. An important step in a shape-only analysis is to subtract the normalization component from the nominal matrix component.

The covariance matrix allows us to account for systematic differences and their correlations in the three detectors and the difference in flux at their locations. This matrix boils down to three main components: uncertainties in the shape of the distribution, those in the normalization, and those in the bin-to-bin normalization ("mixed component"). Components of our nominal uncertainty matrix can be factorized into the following equations [7]:

$$E_{ij}^{shape} = E_{ij} - \frac{N_j}{N_T} \sum_{k=1}^{n} E_{i,k} - \frac{N_i}{N_T} \sum_{k=1}^{n} E_{k,j} + \frac{N_i N_j}{N_T^2} \sum_{kl}^{n} E_{k,l}, \tag{4}$$

$$E_{ij}^{mixed} = \frac{N_j}{N_T} \sum_{k=1}^{n} E_{i,k} + \frac{N_i}{N_T} \sum_{k=1}^{n} E_{k,j} - 2\frac{N_i N_j}{N_T^2} \sum_{kl}^{n} E_{k,l}, \text{ and} \tag{5}$$

$$E_{ij}^{norm} = \frac{N_i N_j}{N_T^2} \sum_{kl}^{n} E_{k,l}. \tag{6}$$

The final result can be seen in Fig. 3.

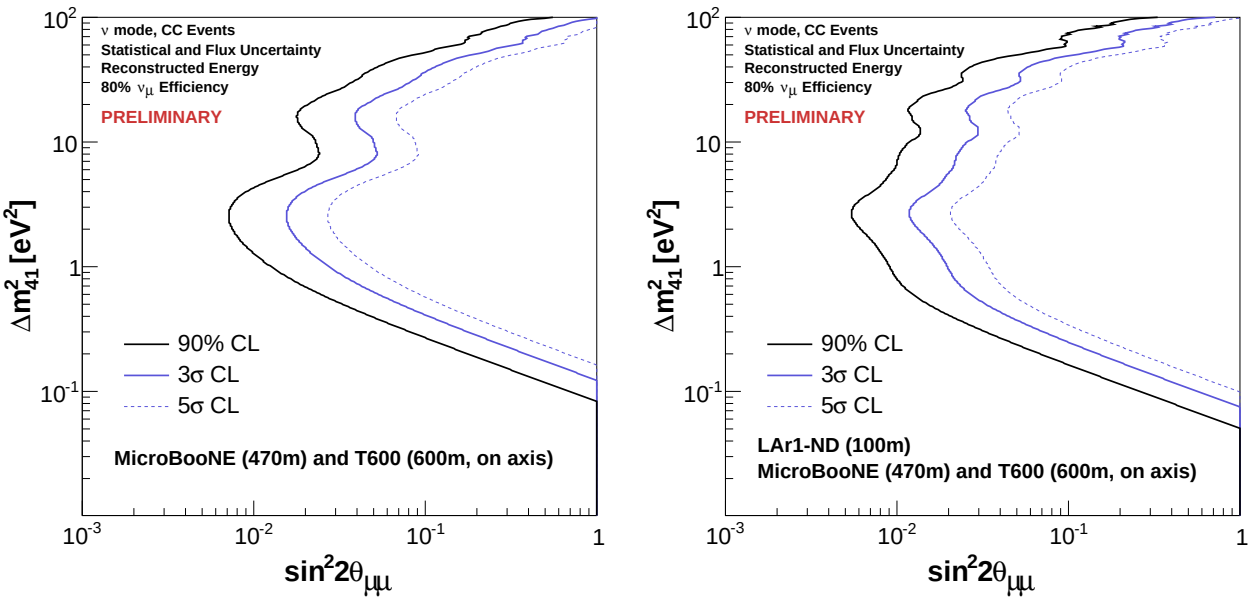

FIG. 3: *Sensitivity curves for different detector setups, including LAr1–ND with an exposure of* 6.6×10^{20} *POT, MicroBooNE, with* 6.6×10^{20} *POT, and T–600, with* 6.6×10^{20} *POT. Contours are drawn around regions of sensitivities greater than* 5σ*,* 3σ*, and* 90% *confidence levels.*

IV. SIGNAL INJECTION

These sensitivity curves illustrate how well signals can be resolved across the phase space. This is useful in demonstrating the power of a detector setup. We want to go a step further and study how well we can constrain the parameters of a single, specific signal.

To do this, we feed an input in the form of a coordinate on the Δm^2_{41}–$\sin^2(2\theta_{\mu\mu})$ plane and a signal vector is created by subtracting the ν_μ spectrum that transitioned to sterile neutrinos of the given parameters from the null hypothesis. Before the χ^2 values are calculated, the prediction vectors are all scaled to match the "real" signal in the near detector. This scaling is done on a bin-by-by basis for each energy spectrum in each detector and it is another consequence of the shape-only analysis, removing all normalization from the comparison. In Fig. 4, we see an example of a signal vector and a prediction vector for another point in the phase space. In the near detector, the contribution to the χ^2 value is zero, so all χ^2 information comes from MicroBooNE and T–600.

The χ^2 values are then calculated using:

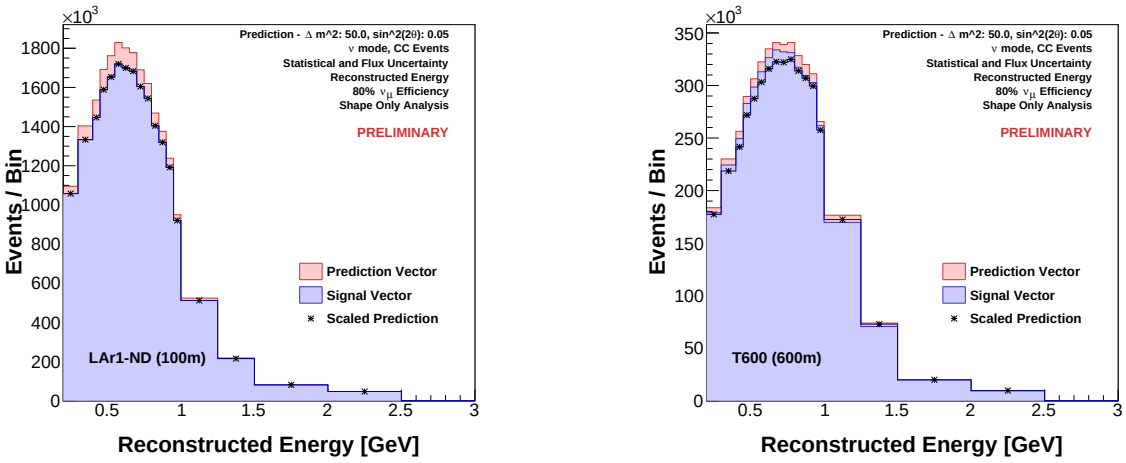

FIG. 4: *Scaling of the muon neutrino disappearance energy distribution in a shape-only signal injection analysis in the near and far detector. The injected signal in each plot has oscillation parameters* $\sin^2(2\theta_{\mu\mu}) = 0.1$, $\Delta m^2_{41} = 10\ eV^2$.

$$\chi^2 = (E_{sig} - E_{pred})_i Cov^{-1}_{ij} (E_{sig} - E_{pred})_j \tag{7}$$

where E_{sig} represents the energy bins for the signal matrix.

With this array of χ^2 values, we must determine the best-fit point. The best-fit is the set of oscillation parameters corresponding to the closest match of prediction to signal. It is where the code believes this injected signal lies in the phase space. The best-fit is found by determining the point on the Δm^2_{41}–$\sin^2(2\theta_{\mu\mu})$ with the lowest χ^2 value. Fig. 5 shows a plot of each χ^2 value over the phase space.

We again run a one-directional Raster scan through the χ^2 values to place our confidence level cuts, but with an altered selection mode. For each point on the Δm^2_{41}–$\sin^2(2\theta_{\mu\mu})$ plane, we decide to mark it for a given confidence level if it satisfies the following inequ ality:

$$\chi^2 \leq \chi^2_{C.L.} + \chi^2_{low}. \tag{8}$$

Where χ^2_{low} is the lowest χ^2 value, or the value corresponding to the best-fit point. While the scan is still one-directional, the contours will be cut at both sides. This way of cutting off the confidence levels also means that we are taking into account both the $\sin^2(2\theta_{\mu\mu})$ and Δm^2_{41} parameters, so we must use a two-sided χ^2 distribution with two degrees of freedom [6]. The software looks for points in the 90% confidence level ($\chi^2_{C.L.} \leq 4.61$), 3σ ($\chi^2_{C.L.} \leq 11.83$) and 5σ

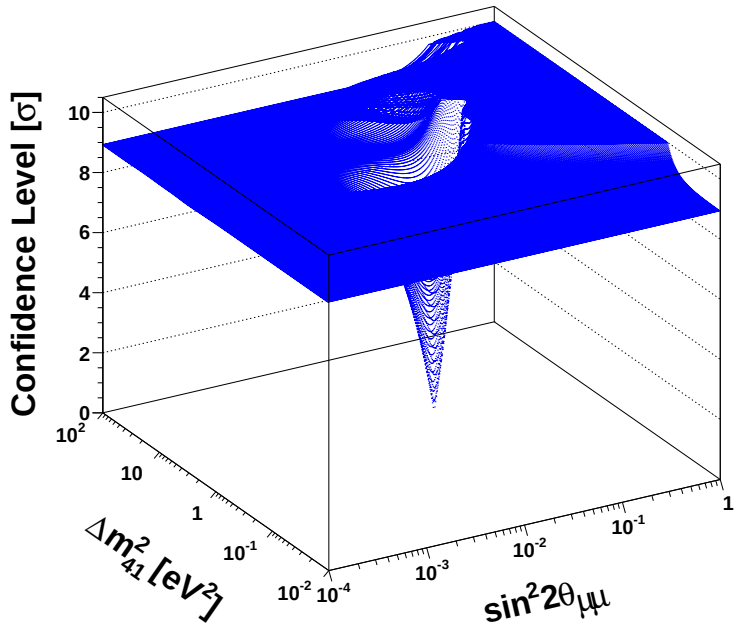

FIG. 5: χ^2 *surface for injected signal of oscillation parameters* $\sin^2(2\theta_{\mu\mu}) = 0.038$ *and* $\Delta m^2_{41} = 0.25$. *The confidence level,* **given by the square root of the** χ^2 **value**, *is shown for each point on the phase space. For display purposes, the confidence level is cut off at* 10σ *(*$\chi^2 = 100$*).*

($\chi^2_{C.L.} \leq 28.23$).

The confidence levels in this plot signify how well we may determine the oscillation parameters of the signal. We see in Fig. 7a that the parameters may be constrained fairly close to the actual signal. In Figs. 7b-7d, we see that as we walk the signal further into the low $\sin^2(2\theta_{\mu\mu})$ and therefore out of the high sensitivity area signified in Fig. 3, we see the allowed regions on the plot grow, making the parameters of oscillation harder to constrain. In the last figure, showing a signal far outside the 5σ region on the signal injection plot, we see that there is no closed contour able to fit on the plane, representing limitations in our ability to constrain parameters in that sector to any high degree of confidence.

At this point, these signal injection plots are incredibly optimistic. Since both the signal and prediction vectors are produced by the same means, the construction of this code dictates that this lowest χ^2 will always be equal to zero and will always line up perfectly with the injected signal.

The solution to this is to introduce random fluctuation based on the statistical uncertainty in the signal to simulate results that might be seen after a limited run by the detectors. The

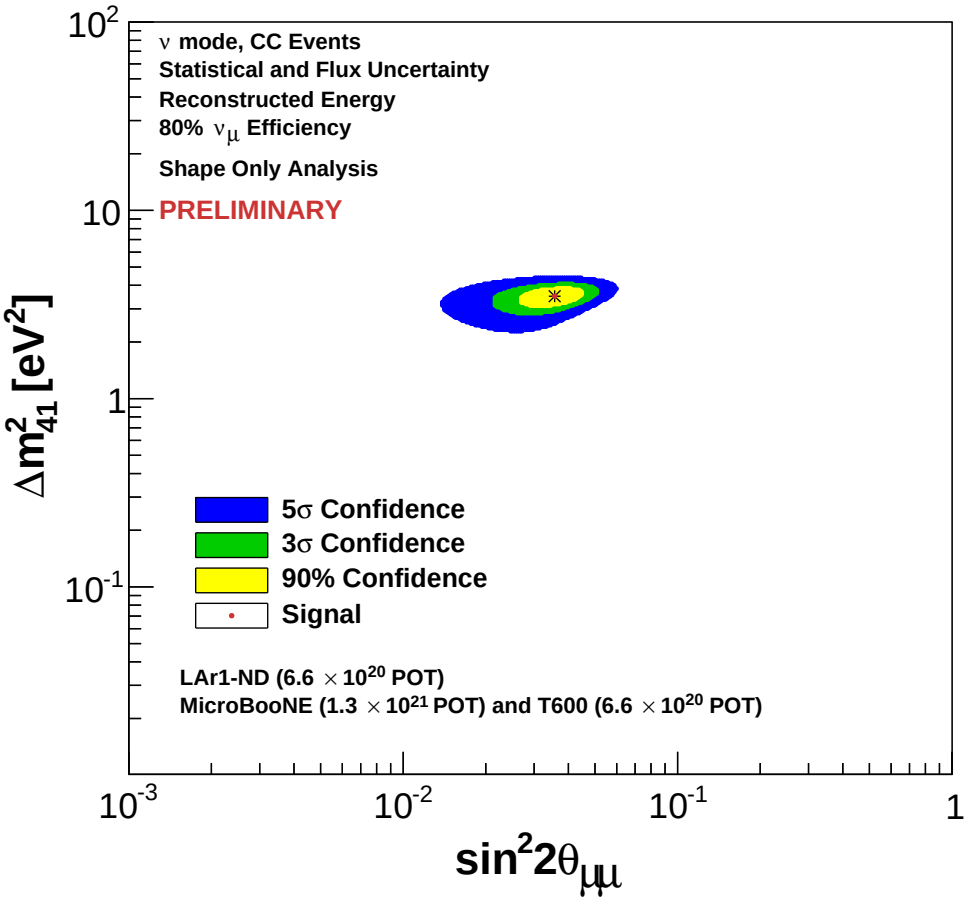

FIG. 6: *Plot of allowed region for injected signal. The yellow region represents constraint of the signal oscillation parameters to a* 90% *confidence level, the green represents constraint to a* 3σ *confidence level and the blue to a* 5σ *confidence level. The best-fit point is marked with a small star.*

signal vector is created exactly as before and then a Poisson distribution is implemented to fluctuate each individual bin. This correspond to a sample of *"fake data"*. Prediction vectors are then scaled to this fluctuated signal and the rest of the calculations proceed as before.

Now that the signal has been given random fluctuations, it no longer represents a perfect match with some corresponding prediction vector. The lowest χ^2 will no longer always be zero, as we see in Fig. 9 which represents the same exact data as in Fig. 5, but with added fluctuation.

Since there is no longer a perfect match for the two vectors, the best-fit point will not necessarily agree with the signal. We need to add one more step to the process. The covariance matrix is originally built without any assumptions about a signal, which is much like a real-life case. The matrix is fractionalized and scaled to a null hypothesis. After a signal is detected,

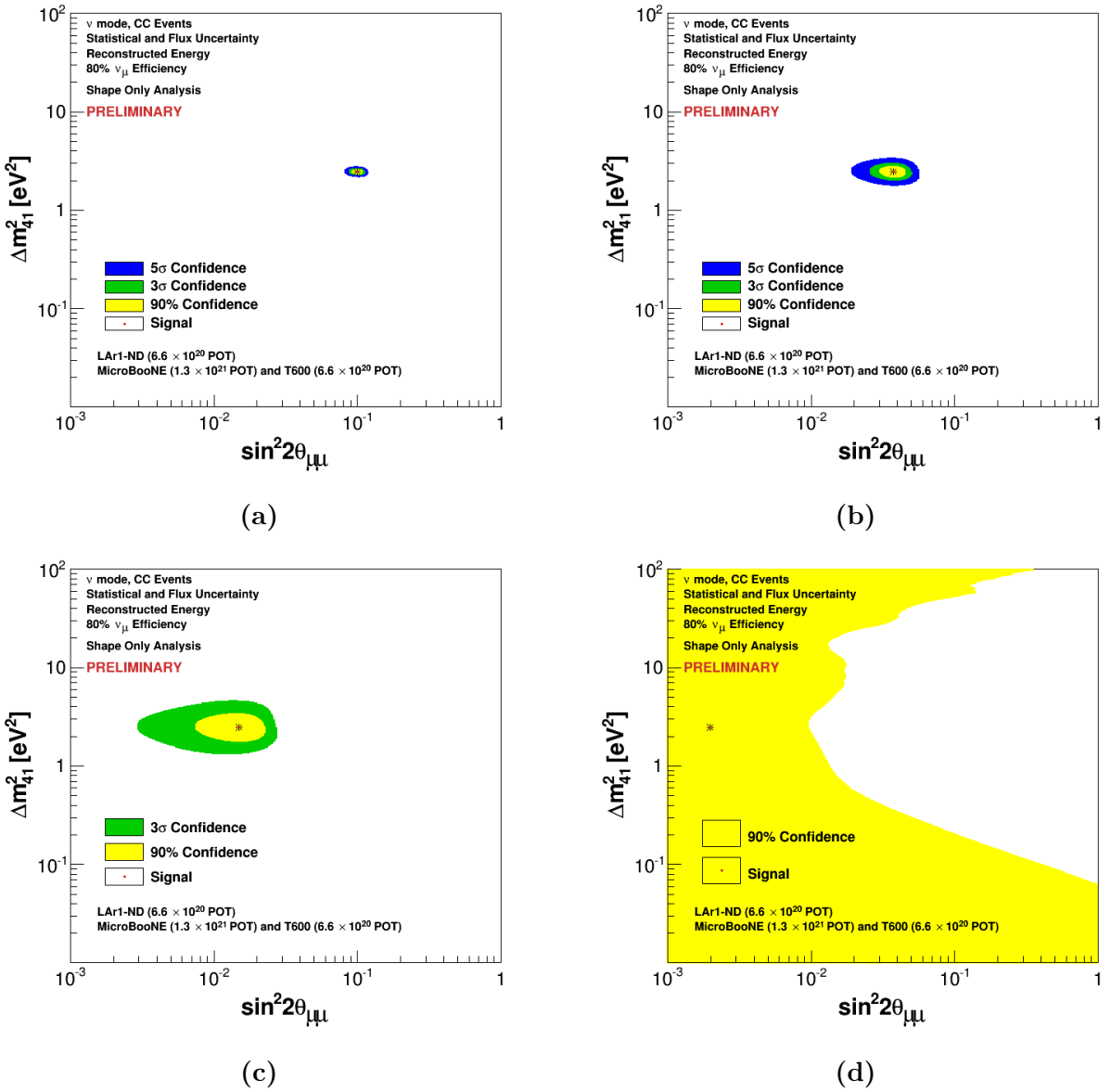

FIG. 7: *Plots of allowed regions for signals at* $\Delta m^2_{41} = 2.5eV^2$, *and a)* $\sin^2(2\theta_{\mu\mu}) = 0.1$, *corresponding to a signal well within the* 5σ *region of the sensitivity plots (see Fig. 3), b)* $\sin^2(2\theta_{\mu\mu}) = 0.038$, *corresponding to a signal within the* 3σ *region of the sensitivity plots, c)* $\sin^2(2\theta_{\mu\mu}) = 0.015$, *corresponding to a signal within the* 90% *confidence level region of the sensitivity plots, and d)* $\sin^2(2\theta_{\mu\mu}) = 0.002$, *corresponding to a signal lying well outside of the* 90% *confidence level region of the sensitivity plots.*

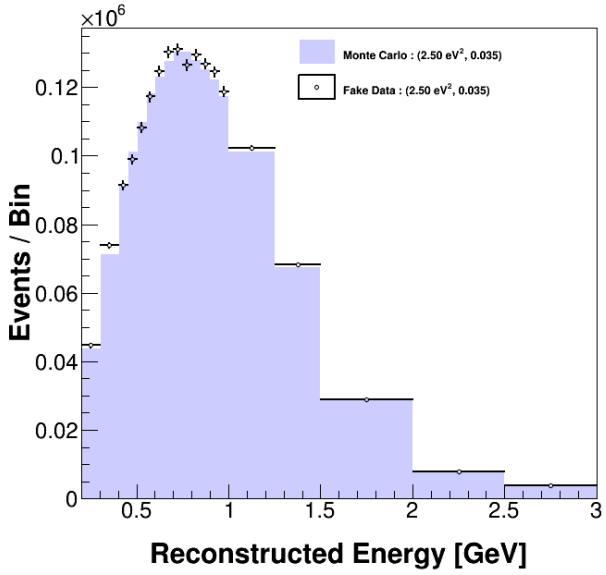

FIG. 8: *Plot of the bin-by-bin Poisson fluctuation of the ν_μ energy spectrum for a signal vector in the far detector.*

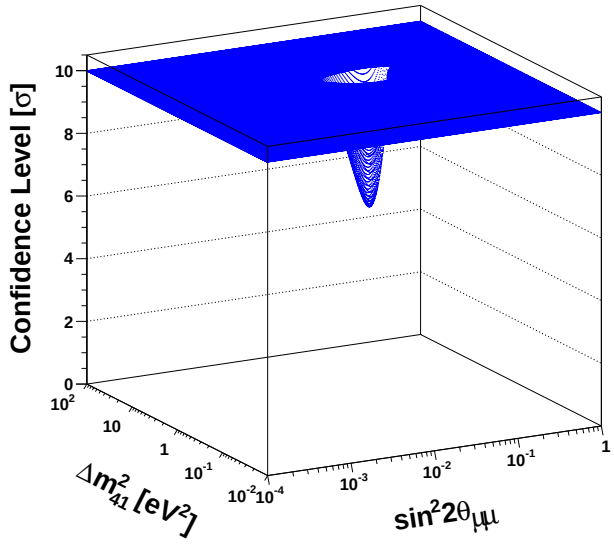

FIG. 9: χ^2 *surface for a fluctuated injected signal.*

however, and a best-fit point is found, this matrix must be updated. The covariance matrix is rebuilt as before, but instead scaled to the best-fit signal.

With the new covariance matrix, the χ^2 values are calculated again and a new best-fit point is found. The code then checks whether or not the χ^2_{min} has changed by more than 0.002 after

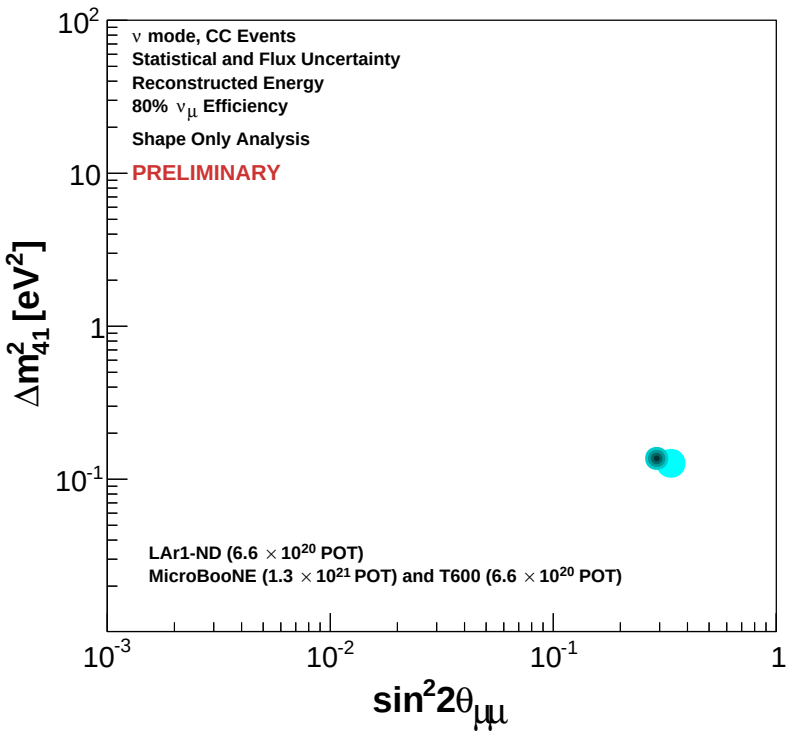

FIG. 10: *The best fit point is plotted after the initial χ^2 calculation and then once more for each of four more iterations. The markers get darker and smaller for each following iteration, but note that we only see significant movement between the markers for the first and second best fits. After the first covariance matrix update, the best fit does not display any movement.*

the matrix rebuild and if it has, then it rebuilds the covariance matrix again, feeding the new best-fit into it. The process repeats until the χ^2 moves by less than 0.002 or ten iterations occur, implying a failure to converge.

In Fig 10, we see a plot of the best fit point after each iteration. We can see that after one iteration, there is a movement of the best fit point, but beyond that, it remains relatively still. The most significant change comes from the first update of the covariance matrix, where the null hypothesis is replaced with some signal.

But there are still problems! The best fit point is inconsistent from one run to another, rarely landing on the actual injected signal despite these iterations. Each time the code is run, it represents a pseudo-experiment and the signal is re-fluctuated. In the high $\sin^2(2\theta_{\mu\mu})$ region where allowed regions are universally very tight this issue is virtually non-existent, but as we move further towards the left of the plot, we see increased instability.

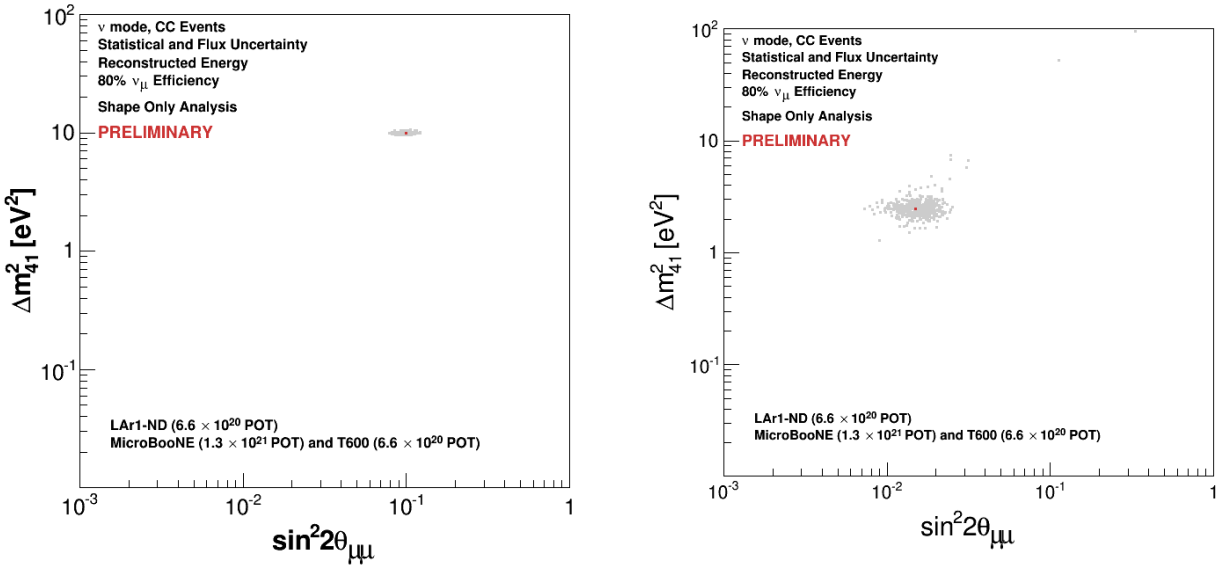

FIG. 11: *Plots of the best fit points after simulating* 500 *pseudo-experiments for two different injected signals. The red point marks the injected signal and each gray point marks the best-fit point from one pseudo-experiment.*

This calls into question to the manner by which we cut confidence levels. The shortcut approach that we employ using a two-sided χ^2 distribution is effective to first order. Once statistical fluctuations are introduced to the signal, it simulates *"fake data"* which presents us with our limitations. Each individual run of the code represents an experiment, so confidence levels can no longer be given by their χ^2 value. A confidence level is defined as a region containing a specific portion of best-fit points after several pseudo-experiments. In order to account for this and draw proper confidence levels, the code would need to be run thousands of times for each injected signal to map regions to the discovered best-fits. As an example of this, Fig. 11 shows the positions of best fit points after 500 pseudo-experiments each.

These plots demonstrate the limitations of the software as the signal is pushed further towards the edges of sensitivity. When the signal is firmly within the 90% confidence contour of the sensitivity plots, all of the best fit points are clustered very close. Once this signal moves out, however, the best-fit may vary wildly with each experiment. Some notable points are those at very high Δm^2_{41}, incredibly far away from the injected signal. If the signal moved to an even lower $\sin^2(2\theta_{\mu\mu})$, we see the plots in Fig.12. The best fit points appear to outline the sensitivity contours and few if any exist very close to the injected signal. Interestingly, there is a distinct imbalance of best-fit plottings, with the points favoring higher values of Δm^2_{41}. This is further illustrated in the shape and rate analysis plot of Fig.12. This weighting towards high Δm^2_{41} comes as a consequence of the nature of the analysis. The Δm^2_{41} component in the

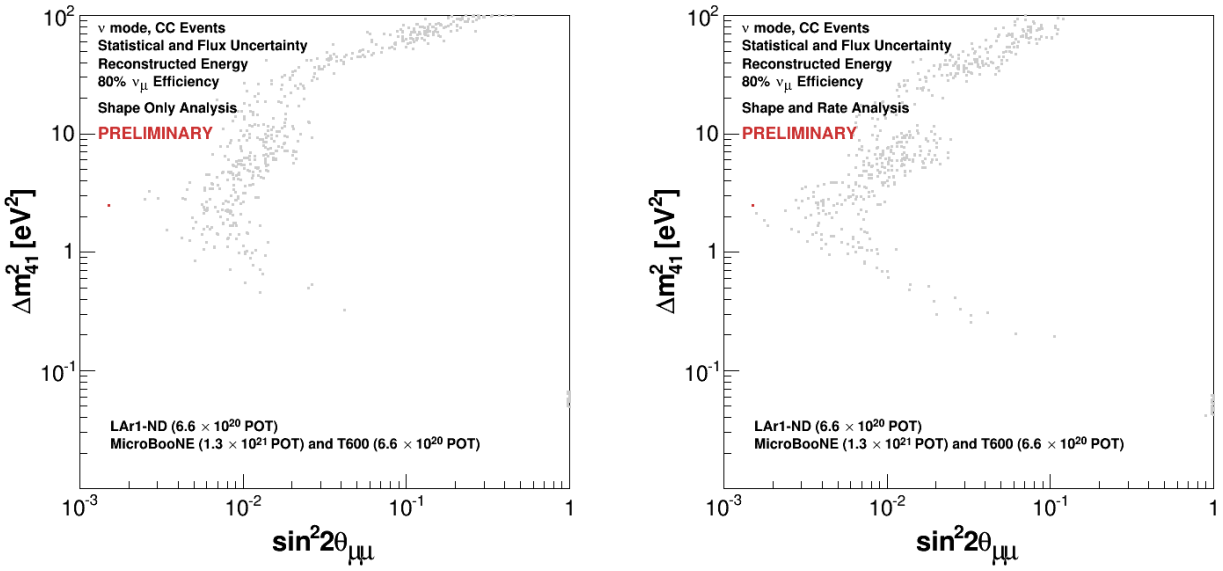

FIG. 12: *Plots of the best fit points after simulating* 500 *pseudo-experiments for the same signal. The red point marks the injected signal and each gray point marks the best-fit point from one pseudo-experiment. One is a shape-only analysis, and the other contains normalizations information, making it a shape and rate analysis.*

neutrino oscillation probability formula corresponds to oscillation frequency. All sufficiently high frequencies will be indiscernible from each other, since the oscillation will approximate to half of the amplitude. For lower Δm^2_{41}, we will see lower, more distinct frequencies, which will present higher χ^2 values when compared to other signals.

V. CONCLUSIONS

These studies show that the detector setup of the Short Baseline Program greatly expands the current limits in ν_μ disappearance studies. The signal injection plots further demonstrate the sensitivities shown in earlier studies while simultaneously presenting the reasoning why these studies are being performed. Further efforts in these studies will need to apply a statistical approach to assigning the confidence level cuts in order to account for the fluctuation of the

best-fit point for signals in low-sensitivity regions of the phase space.

---

[1] A. A. Aguilar-Arevalo *et al.* [MiniBooNE Collaboration], Phys. Rev. Lett. **110**, 161801 (2013) [arXiv:1207.4809 [hep-ex], arXiv:1303.2588 [hep-ex]].

[2] A. Aguilar-Arevalo *et al.* [LSND Collaboration], Phys. Rev. D **64**, 112007 (2001) [hep-ex/0104049].

[3] A. A. Aguilar-Arevalo *et al.* [MiniBooNE Collaboration], Phys. Rev. D **81**, 092005 (2010) [arXiv:1002.2680 [hep-ex]].

[4] A. A. Aguilar-Arevalo *et al.* [MiniBooNE Collaboration], Phys. Rev. D **79**, 072002 (2009) [arXiv:0806.1449 [hep-ex]].

[5] D. W. Schmitz, "A measurement of hadron production cross sections for the simulation of accelerator neutrino beams and a search for ν_μ to ν_e oscillations in the δm^2 about equals $1 - eV^2$ region," FERMILAB-THESIS-2008-26.

[6] M. Shaevitz, "Chi2 vs Confidence Level Cut Values," MicroBooNE Document 3697 (2014).

[7] M. Shaevitz, "Separating components of error matrices," BooNE Technical Note 253.

[8] K. Mahn, T. Katori, S. Brice,"Eventweight and multisimmatrix: a guide to the reweighting and MiniBooNE error analysis with multisims," BooNE Technical Note 231.